Progress In Electromagnetics Research C, Vol. 100, 187–203, 2020

A Metamaterial Loaded Hybrid Fractal Hepta-Band Antenna for Wireless Applications with Reconfigurability Characteristics

Santosh Kumar Dwivedi*, Mithilesh Kumar, and Lokesh Tharani

Abstract—In this article, the authors present a hepta band metamaterial inspired hybrid fractal octagonal shape antenna for wireless applications. Multiband characteristics in the proposed design are achieved by hybrid fractal form of Moore curve and Koch curve with metamaterial loading. A well matched impedance bandwidth ($S_{11} \leq -10\,\text{dB}$) is accomplished at seven microwave frequency bands, Upper L band ($1.93 \sim 2.08\,\text{GHz}$), S band, WiMAX ($3.3 \sim 3.7\,\text{GHz}$), C band, WLAN ($5.4 \sim 5.9\,\text{GHz}$), C band, IEEE INSAT application ($6.5 \sim 7.2\,\text{GHz}$), X band terrestrial broadband, space communication and Radio Navigation (RN) application ($8.51 \sim 11.05\,\text{GHz}$), Lower Ku band direct broadcast satellite service ($12.2 \sim 12.7\,\text{GHz}$), and Middle Ku band satellite communication operating band ($14.73 \sim 15.84\,\text{GHz}$) covering various wireless applications. The antenna achieves hexa/penta band characteristics during switching ON/OFF state of PIN diode placed between the Moore curve structure (attached with centered SRR cell) and feedline. Radiation patterns are found in stable forms at all the resonant frequencies. Measured results of the proposed design are compared with simulated ones indicating good agreement between them.

1. INTRODUCTION

1.1. Motivation

In recent years, metamaterial loaded multiband antennas with wireless communication capabilities have received widespread attention. Early researches on multiband antennas are focused on wireless applications WLAN/WiMAX. Such multiband antennas represent the facility to integration of various communication standards within single antenna design. To meet the objective of multiband operation within single antenna design without affecting the other antenna parameters is a crucial task. The multiband nature is omitted by implementation of fractal approach, creating slots in ground and radiating area, feeding techniques, etc. Adopting any one of the techniques or hybrid of these techniques can construct the base of design evolution of multiband antennas for covering wireless communication applications. Presently, metamaterial loaded multiband antennas have gained significant attention due to improvement in antenna parameters such as radiation efficiency, bandwidth enhancement, and antenna gain. Incorporating slot/fractalization/metamaterial loading techniques in antenna design can achieve multiband characteristics without much more affecting the antenna parameters. Presently, multi-resonance antennas with frequency band reconfigurability characteristics have gained more attention for wireless communication systems. The feature of reconfigurability is achieved by implementation of PIN diodes in radiating patch area or ground plane without affecting antenna characteristics significantly.

Received 12 January 2020, Accepted 10 March 2020, Scheduled 25 March 2020
* Corresponding author: Santosh Kumar Dwivedi (santoshdwivedi4@gmail.com).
The authors are with the Department of Electronics Engineering, Rajasthan Technical University, Kota, India.

1.2. Related Literature Survey

The progress of multiband technology has risen rapidly through various services. This means that users of smart phones require multiband characteristics to operate at various wireless standards. Some technologies are available to meet the requirement of multiband operation in antenna for wireless communication applications, such as feeding methods [1–3], etching slots on radiating patch or ground plane [4–9], metamaterial inspired techniques [10–14], introducing multi-branched strips, and fractal approach [15]. Implementation of etching slot techniques in antenna design obtains additional resonating bands since slots are responsible for creating electric current perturbation. Single open slot antenna structure is proposed operating on smartphone applications LTE/WWAN [16]. In [17, 18], multiband characteristics are achieved by adopting the etching slot approach to cover varied wireless applications.

Recently, metamaterial inspired multiband antenna cumulates significant attention in smart antenna design because of specific properties of metamaterial, such as negative index of refraction, miniaturization (electrically small), opposite nature of phase and group velocity. Such types of properties support optimum bandwidth, size miniaturization, improved radiation efficiency, and multiband operation in metamaterial loaded antenna. Various designs dedicated to metamaterial loaded multiband antennas have been published [19–21]. In [19], a metamaterial inspired triple band antenna is proposed for WLAN/WiMAX wireless applications. In [20–22], multiple resonating bands are obtained by implementing SRR structure within radiating patch. In [23], the approach of etching slot, fractalization, and metamaterial loading is adopted to focus on the antenna performance regarding size miniaturization, number of resonating bands, and bandwidth enhancement. The hybrid formation of metamaterial and fractal geometry for antenna design is helpful to attain the improvement in impedance matching, gain, radiation efficiency, number of operating bands, and bandwidth [24–26]. In [27], an antenna design consisting a fractal radiating patch with SRR shape ground is proposed to cover various wireless applications. Ref. [28] explains the design of a fractal antenna with Minkowski curve loaded with metamaterial cells to achieve bandwidth enhancement. In [29], researchers report an antenna design showing gain improvement and size reduction by implementation of SRR. A metamaterial inspired compact open split ring resonator (OSRR) antenna is proposed with 38.83% antenna size reduction for Multiband Operation (WLAN/Wi-MAX/X-band) [30]. A multi-resonance antenna loaded with SRR shows reconfigurable nature with the implementation of switching element (RF diode) for wireless standards [31–33]. DGS (defected ground structure) process is derived to create multiple operating bands for wireless applications [34].

This paper presents a part of a research that focuses on the design analysis of a hybrid fractal slot antenna loaded with three metamaterial cells, operating over the wireless applications Upper L band (Satellite navigation), WiMAX, WLAN, C band IEEE INSAT application, X (terrestrial broadband, space communication and Radio Navigation (RN) application), Lower Ku band (direct broadcast satellite service), and Middle Ku band (satellite communication operating band). The proposed structure generates operating bands 1.93–2.08 GHz (7.48%), 2.84–4.43 GHz (43.74%), 5.49–5.90 GHz (7.19%), 6.80–7.77 GHz (13.32%), 8.51–11.05 GHz (25.97%), 12.24–12.73 GHz (3.92%), and 14.73–15.84 GHz (7.26%) in simulation mode and 1.89–2.10 GHz (10.53%), 3.42–3.61 GHz (5.41%), 5.25–6.18 GHz (16.27%), 6.76–7.92 GHz (15.8%), 9.24–10.89 GHz (16.39%), 12.04–12.71 GHz (5.41%), and 14.87–15.76 GHz (5.81%) during experimental mode at wireless standards Upper L band (1.98 GHz), S band WiMAX (3.5 GHz), C band WLAN (5.8 GHz), C band IEEE INSAT application (6.97 GHz), X band (10.34 GHz), Lower Ku band direct broadcast satellite service (12.54 GHz), and Middle Ku band satellite communication operating band (15.23 GHz), respectively. During design evolution process, firstly inserting the hybrid fractal geometry (Moore curve and Koch curve) inside the circular slotted radiating patch area yields three resonant bands at WiMAX, X band, and middle Ku band. Afterward, implementing three SRR cells within radiating portion creates additional four resonant bands which cover the wireless modes Upper L band, WLAN, C band IEEE INSAT application, and Lower Ku band. Placing PIN diode at the strip connected between Moore curve (attached with centered SRR cell) and feedline obtains the frequency band reconfigurability between the wireless standards. During ON/OFF state of PIN diode, the structure resonates in hepta/penta operating band mode, respectively. The surface electrical current length is improved in the case of ON state of diode as compared to OFF state of diode, which is responsible for variation in input impedance, and the structure exhibits two additional operating bands at 1.98 GHz (Upper L band) and (12.54 GHz (Lower Ku band) [35].

The formation of this paper is as follows. First, the design evolution of the hybrid fractal slotted multiband antennas loaded with metamaterial cells is discussed. The design analysis of the proposed hybrid fractal geometry and metamaterial SRR is described thereafter. A section concerning the result analysis of the proposed SRR and its effect on antenna performance follows. Finally, manufacture and test are discussed.

1.3. Novelty of Proposed Design

This section is organized in such a manner; (i) hybrid fractal formation is applied with a slotted patch antenna to obtain multiband operation; (ii) the hybrid fractal geometry is implemented with SRR cells on the radiating portion to obtain hepta operating band characteristics; (iii) various antenna parameters are discussed, such as gain, efficiency, patterns (co- and cross-polarization modes), and current distribution, and these parameters are compared with previous published antenna parameters in tabulation form; (iv) the hybrid fractal radiating geometry adjoined with PIN diode is studied to derive the reconfigurability characteristics of the antenna design for wireless standards. Finally, the outcome of the proposed work is concluded.

2. ANTENNA DESIGN AND CONFIGURATION

This section focuses on design analysis of the proposed metamaterial hybrid fractal multiband antenna. Figures 1 and 2 present design steps of the proposed structure and their respective simulated S_{11} of the configured antenna, respectively. The antenna structure is printed on FR4 substrates of 1.6 mm thickness. Relative dielectric constant of FR4 substrate used is 4.4, and the tangent of loss angle is 0.02. The size of the proposed structure is 29.5 mm × 22 mm × 1.6 mm. From Figure 1, design step-I represents an octagonal shape radiating patch fed with a trapezoidal microstrip line covering UWB single mode. Next, design step-II creates a circular slot inside the radiating patch and the hybrid fractal geometry (fused form of Ist iteration Moore and Koch curve) to derive the multiband characteristics at resonant bands at 3.2/9.6/15.3 GHz, as illustrated in Figure 1 (design step-II) and Figure 2. The circular slot and fused form of hybrid fractal radiating structure are responsible for creating triple operating bands 2.94–3.61 GHz (middle S band), 8.44–10.86 GHz (middle X band), and 14.92–15.71 GHz (middle Ku band). The respective slot and fused hybrid fractal radiating part provide the current perturbation in antenna structure that derives the triple band characteristics. As per the design evolution, step-III is a upgraded form of configuration II, implementing two SRR cells with radiating element to achieve additional operating bands, represented as the six resonant band at Middle S (3.2 GHz), WLAN (5.8 GHz), Upper C (7.3 & 7.8 GHz), Lower X (9.1 GHz), and Middle Ku (15.2 GHz) band. In the case of design step-III, proposed SRR cell loaded with radiating patch portion is liable to generate the additional narrow WLAN band 5.69–5.97 GHz. The solenoidal conducting current will flow in SRR rings which is responsible for obtaining the magnetic response (negative permeability characteristics). Subsequently, by loading the third SRR cell attached with the feedline via Moore curve shape strip line with PIN diode inside it (ON state mode), the hepta band configuration is accomplished covering the wireless standards at Upper L

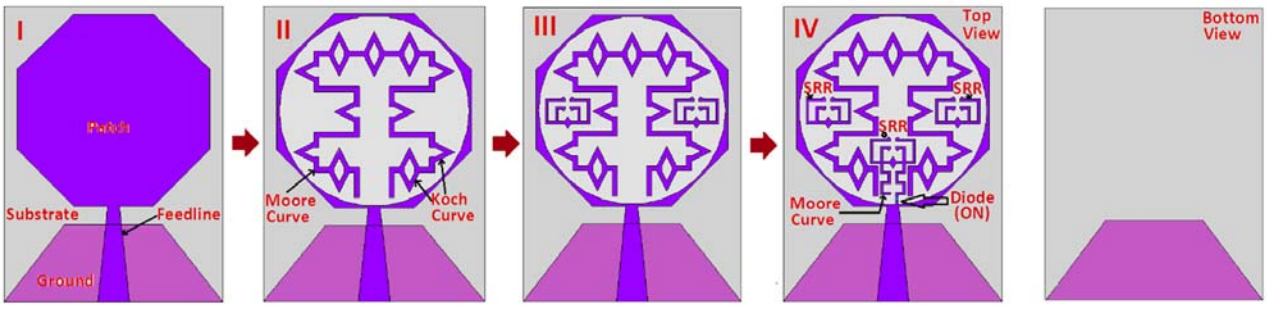

Figure 1. Design steps of proposed configured antenna.

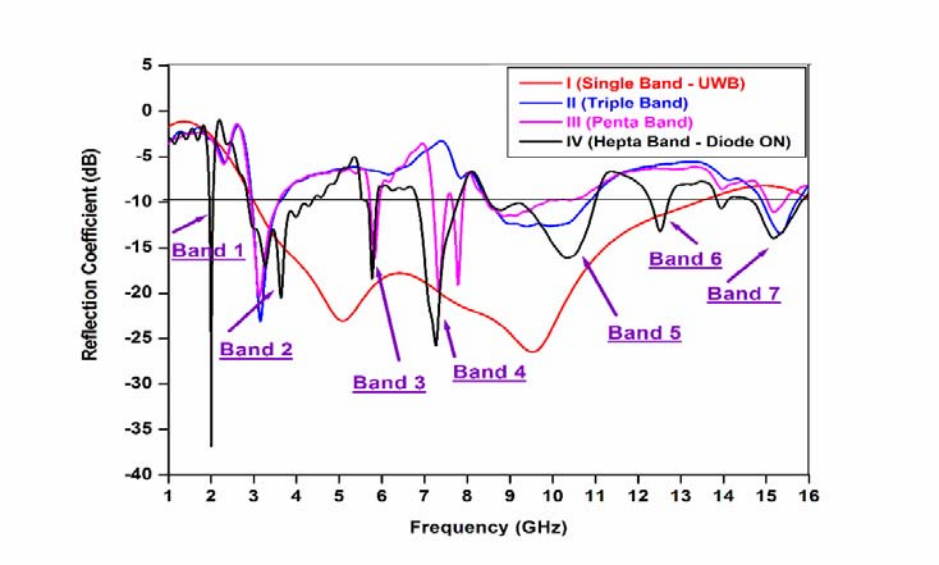

Figure 2. Simulated S_{11} of proposed configured antenna for each design step.

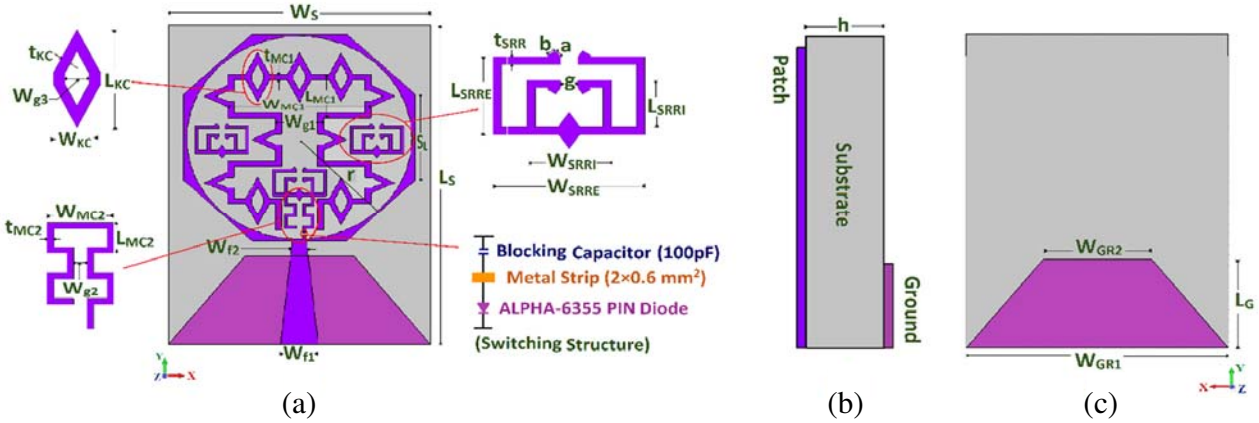

Figure 3. Configured proposed design: (a) Top view, (b) side view, (c) bottom view.

band (1.9 GHz)/S band WiMAX (3.5 GHz)/C band WLAN (5.8 GHz)/C band IEEE INSAT application (6.98 GHz)/X band terrestrial broadband, space communication and Radio Navigation (RN) application (10.35 GHz)/Lower Ku band direct broadcast satellite service (12.5 GHz)/Middle Ku band satellite communication operating band (15.2 GHz), as represented in proposed design step-IV of Figure 1 and Figure 2. In design step-IV, during ON state of PIN diode an effect of current perturbation in antenna design is created which leads to the hepta band configuration [36, 37].

As per design step-IV, the final configured antenna is fabricated on an FR4 substrate with electrical dimension $0.191\lambda \times 0.142\lambda \times 0.0103\lambda$ (29.5 mm × 22 mm × 1.6 mm) at lower frequency of 1.94 GHz fed by a trapezoidal shape feedline (characteristic impedance of 50 ohm), as shown in Figure 3. The proposed design consists of a radiating part of a circular slot (radius 9.45 mm) with hybrid fractal geometry loaded with three SRR cells and trapezoidal shape ground plane, as indicated in Figures 3(a) and (c). The proposed hybrid fractal part is made by fusion process of Ist iterated Moore curve with 0th iterated Koch curve. Metamaterial SRR cells are designed on a dielectric substrate FR4 having two rectangular (flared at edges) rings connected commonly at one side and opened at the opposite side. The top, side, and bottom views of the proposed configured antenna are shown in Figure 3. The parametric values (in mm) of the proposed structure are: $L_S = 29.5$, $W_S = 22$, $h = 1.6$, $r = 13$, $S_L = 8$, $W_{f1} = 3.16$, $W_{f2} = 1.2$, $W_{GR1} = 22$, $W_{GR2} = 10$, and $L_G = 8$. The simulation and fabrication process of the proposed design is carried out by using transient solver of simulator CST Microwave Studio (MWS-version 2014) [38]

and PCB prototype machine, respectively. The upper and lower parts of the fabricated prototype are indicated in Figure 4.

The biasing operation of PIN diode is done by using the DC voltage source applied across the rectangular shape conducting strip having size $2 \times 0.6\,\text{mm}^2$. The respective strip, PIN diode, and blocking capacitor of 100 pF are connected in series and placed between the moore curve strip and feedline as shown in Figure 3(a). A blocking capacitor provides the facility of RF connection to the diode and also works as an isolator for dc signal. Here the beam lead PIN diode ALPHA-6355 is used to generate the reconfigurability characteristics in design and represents $2.6\,\Omega$ resistance and 0.081 pF capacitance during ON and OFF mode respectively by applying the DC voltage (0.7 Volt) [39]. The equivalent circuit of PIN diode for ON/OFF state indicates the series/shunt combination of R_{CC} (resistor)/L_F (fixed value inductor)/C_R (reactive capacitor) as illustrated in Figure 5.

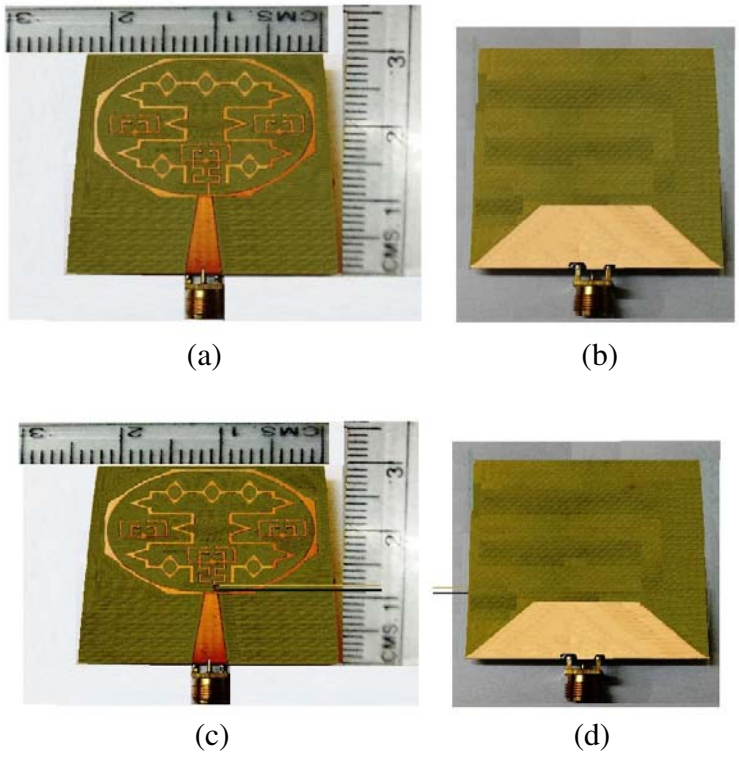

Figure 4. Printed prototype: (a) Upper part (without diode); (b) lower part (without diode); (c) upper part (with diode); (d) lower part (with diode).

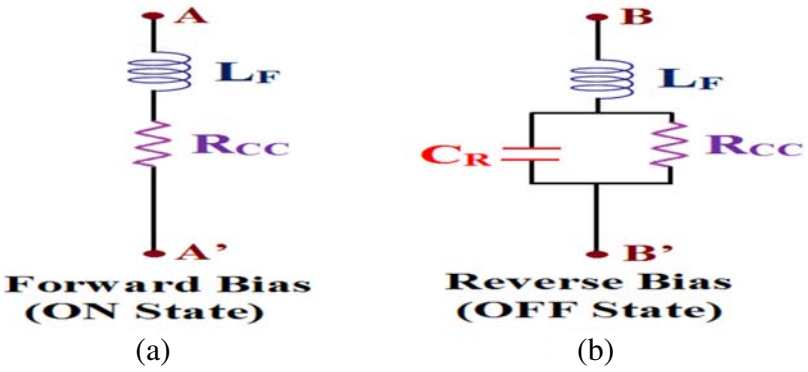

Figure 5. PIN diode RF-equivalent circuit.

Figure 6. Measurement setup (anechoic chamber with VNA) for proposed antenna.

As mentioned, the measurement setup in Figure 6 shows the experimental S_{11} and radiation gain/efficiency/patterns with the help of vector network analyzer (VNA) and anechoic chamber. From Table 1, in the case of OFF state of PIN diode, structure resonance on five operating bands because of the electrical current length is reduced whereas during ON state of diode, the antenna covers the hepta band characteristics due to larger current path (as shown in Figure 7). The proposed configured antenna represents the hepta operating bands (by changing the mode of PIN diode from OFF mode to ON mode) with impedance bandwidth of 7.48% (1.93–2.08 GHz), 43.74% (2.84–4.43 GHz), 7.19% (5.49–5.90 GHz), 13.32% (6.80–7.77 GHz), 25.97% (8.51–11.05 GHz), 3.92% (12.24–12.73 GHz), and 7.26% (14.73–15.84 GHz) in simulation process and 10.53% (1.89–2.10 GHz), 5.41% (3.42–3.61 GHz), 16.27% (5.25–6.18 GHz), 15.8% (6.76–7.92 GHz), 16.39% (9.24–10.89 GHz), 5.41% (12.04–12.71 GHz), and 5.81% (14.87–15.76 GHz) during measurement process as illustrated in Figure 7. It is noticed that the proposed multiband antenna acquires sufficient bandwidth to fulfill the necessity of various wireless applications.

Table 1. Frequency band reconfigurabilty for forward/reverse bias mode of PIN diode.

Diode States	Operating range (in GHz)		10-dB bandwidth (in %)		No. of resonant bands
	Sim.	Exp.	Sim.	Exp.	
Forward Bias (ON Mode)	1.93–2.08/ 2.84–4.43/ 5.49–5.90/ 6.80–7.77/ 8.51–11.05/ 12.24–12.73/ 14.73–15.84	1.89–2.10/ 3.42–3.61/ 5.25–6.18/ 6.76–7.92/ 9.24–10.89/ 12.04–12.71/ 14.87–15.76	7.48/43.74/ 7.19/13.32/ 25.97/3.92/ 7.26	10.53/5.41/ 16.27/15.8/ 16.39/5.41/ 5.81	7-Bands (Upper L band — 1.98 GHz/ S band WiMAX — 3.5 GHz/ C band WLAN — 5.8 GHz/ C band IEEE INSAT application — 6.97 GHz/ X band — 10.34 GHz/ Lower Ku band direct broadcast satellite service — 12.54 GHz/ Middle Ku band satellite communication operating band — 15.23 GHz)
Reverse Bias (OFF Mode)	2.91–3.62/ 5.48–5.86/ 6.82–7.63/ 9.54–11.14/ 14.94–15.73	3.14–3.59/ 5.62–5.85/ 6.89–7.58/ 9.62–10.92/ 14.98–15.54	21.75/6.70/ 11.21/15.47/ 5.15	13.37/4.01/ 9.54/12.66/ 3.67	5-Bands (S band WiMAX — 3.5 GHz/ C band WLAN — 5.8 GHz/ C band IEEE INSAT application — 6.97 GHz/ X band — 10.34 GHz/ Middle Ku band satellite communication operating band — 15.23 GHz)

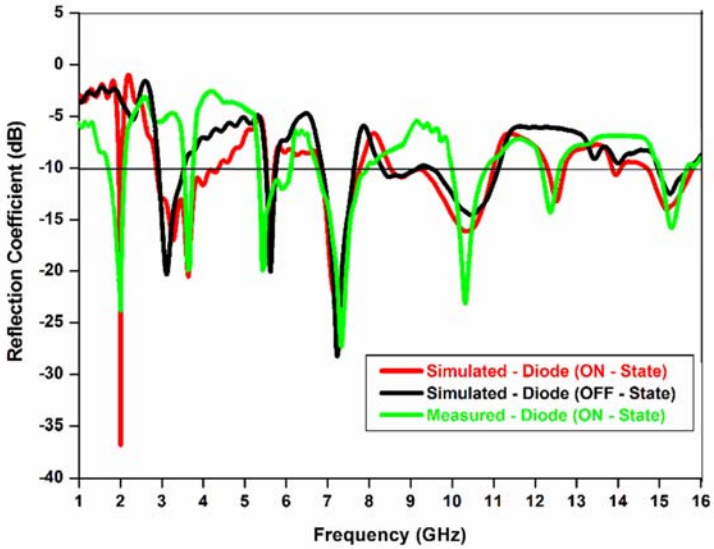

Figure 7. S_{11} versus frequency observation in simulated and measurement mode.

2.1. Study of Hybrid Fractal Geometry

The proposed hybrid fractal geometry is formed by implementation of two different fractal curves. Fractalization of the curve is obtained by repetition of itself with a constant factor in iteration stages. Finalized hybrid fractal form is derived with the help of the Iterative Function System (IFS). The expressions of the fractal dimension (D_{fr}) and length (L_{fr}) are represented in the Equations (1) and (2) [40].

$$D_{fr} = \log(T_s)/\log(e_i) \tag{1}$$

$$L_{fr} = h_c(T_s/e_i)^n \tag{2}$$

where

T_s = Number of segment

e_i = Number of segment partitioning on iteration

h_c = Curve height

n = Number of iteration stages.

The IFS approach is based on mathematical analysis used to design the fractal structures and implement the affine transformation to an elementary shape. Such transformation performs the scaling, translation, as well as rotation, indicated in equations below [40];

$$P(x) = AX + Tr = \begin{bmatrix} a1 & a2 \\ a3 & a4 \end{bmatrix} \begin{bmatrix} x1 \\ x2 \end{bmatrix} + \begin{bmatrix} \text{tr1} \\ \text{tr2} \end{bmatrix} \tag{3}$$

$$A = \frac{1}{q} \begin{bmatrix} \cos\theta' & -\sin\theta' \\ \sin\theta' & \cos\theta' \end{bmatrix} \tag{4}$$

where

A = Initial geometry matrix

$a1, a2, a3, a4$ = Rotation and scaling controlling parameters

$x1, x2$ = Coordinate point of X

tr1, tr2 = Translation and linear shift factor controlling parameters

q = Scaling factor

θ' = Rotation angle factor

Tr = Translation factor.

To achieve the proposed hybrid fractal geometry, implement the Hutchinson operator $H(A)$ on the set of transformation of 'A' represented in Equation (5) [40];

$$H(A) = U_{n=1}^{N} H_n(A) \tag{5}$$

The proposed hybrid fractal antenna is designed by fusion 1st iterated form of the Moore-Koch curve, as shown in Figure 8. In design, 1st iterated Moore curve is considered as an initiator, and 1st iterated Koch curves (double sided — upper and below) as a generator are superimposed on each segment of the initiator curve as illustrated in Figures 8(a)–(c). From Figure 8(c), it is observed that the length of the radiating conducting section increases about 48% as Koch curve is superimposed on Moore curve (six segments — single upper sided and five segments — double sided upper and below form). Initially, the length of base Moore curve is 70 mm without fusion of the Koch curve which increases up to 141.68 mm when Koch curve is integrated with Moore curve. The optimized parametric dimensions (in mm) of proposed hybrid fractal structure are (from Figure 3): $L_{MC1} = 4$, $W_{MC1} = 12$, $t_{MC1} = 0.5$, $W_{g1} = 4$, $L_{MC2} = 1$, $W_{MC2} = 2.5$, $t_{MC2} = 0.25$, $W_{g2} = 0.5$, $L_{KC} = 4.5$, $W_{KC} = 2$, $t_{KC} = 0.5$, and $W_{g3} = 1$.

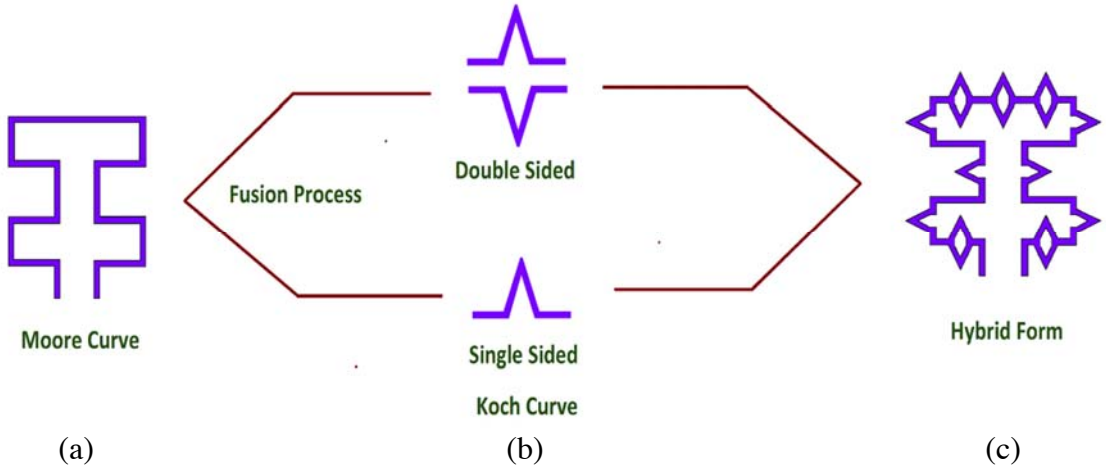

Figure 8. (a) 1st iterated Moore curve, (b) 1st iterated Koch curve, (c) proposed hybrid fractal geometry (integrated Moore-Koch curve).

2.2. Study of Metamaterial SRR

This section presents the design methodology of the proposed magnetic metamaterial SRR cell. SRR cell consists of the modified rectangular shape metallic rings (resonator) flared at corners with split gap, as indicated in Figure 9. The waveguide setup is formed to obtain S-parameters (S_{11} and S_{21}) to retrieve the effective permeability (μ_{eff})/permittivity (ε_{eff}) of the proposed SRR cell. Figure 9 represents the setup in simulation mode with the help of simulator CST Microwave Studio (MWS-version 2014) and equivalent formation of proposed SRR [38]. Experimental S parameters are generated by putting the SRR geometry inside the waveguide environment with two coaxial-to-waveguide adapters and VNA [41]. The parametric values (in mm) of the proposed SRR structure are (from Figure 3): $L_{\mathrm{SRRE}} = 2.5$, $W_{\mathrm{SRRE}} = 4.5$, $L_{\mathrm{SRRI}} = 1.5$, $W_{\mathrm{SRRI}} = 2.5$, $t_{\mathrm{SRR}} = 0.25$, $g = 0.5$, $a = 0.66$, and $b = 0.61$.

Whenever the H field (external) is applied across the SRR, an EMF is generated, which is coupled with the two metallic rings. In this situation, current is flowing from outer to inner ring through the ring spacing (Gap between the conducting rings = g') responsible for creating the distributed capacitance. Therefore, the entire geometry represents the LC resonant characteristics. The resonant frequency of

the proposed SRR cell is evaluated by using [42],

$$f_r = 1/[2\pi \mathrm{SQRT}(L_{\mathrm{teq}} C_{\mathrm{teq}})], \tag{6}$$

where

$$L_{\mathrm{teq}} = 0.0002\,[\{2(L_{\mathrm{Extr}} + W_{\mathrm{Extr}}) - g)\}\,\{\log_e 8(L_{\mathrm{Extr}} + W_{\mathrm{Extr}} - 0.5g)/t\} - J] \tag{7}$$

$$C_{\mathrm{teq}} = 1/2\left[\left\{(L_{\mathrm{Extr}} + W_{\mathrm{Extr}}) - \pi(t + 0.5g') - g\right\}\left\{(0.3\times 10^{-8})(\mathrm{SQRT}(\varepsilon_e))/Z_0\right\} + \left\{(8.85\times 10^{-12})ht/g\right\}\right] \tag{8}$$

where L_{teq} = Total equivalent inductance, C_{teq} = total equivalent capacitance, L_{Extr} = Length of External conducting ring of SRR, W_{Extr} = Width of External conducting ring of SRR, $g_2 = g_1 = g$ = Split gap of conducting ring of SRR, $t_2 = t_1 = t$ = Thickness of External conducting ring of SRR, J = Constant (fixed value = 2.451), g' = Gap between the conducting rings, ε_e = Effective permittivity of the medium, Z_0 = Characteristic impedance, h = Height of the conducting strip.

The effective medium parameter (permeability ($\mu_{effecti}$)) is obtained by using the following equation [43–45]:

$$\mu_{effecti} = n_{ref} \times z_s \tag{9}$$

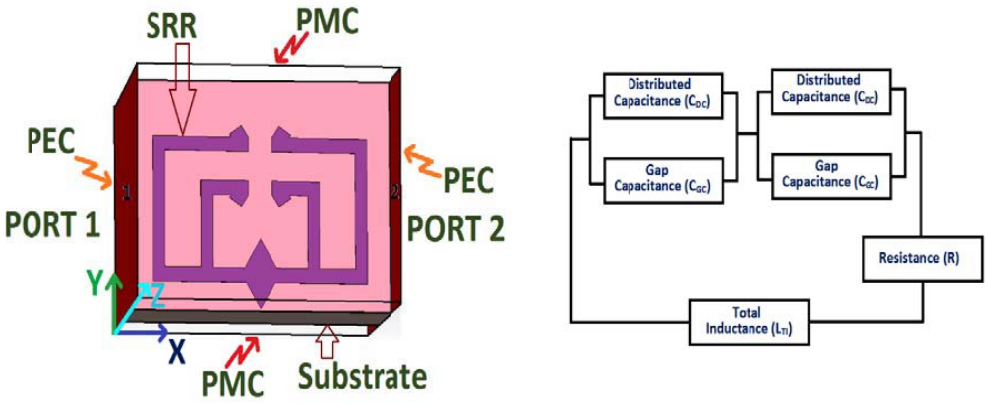

Figure 9. Waveguide setup (simulation mode) with equivalent circuit.

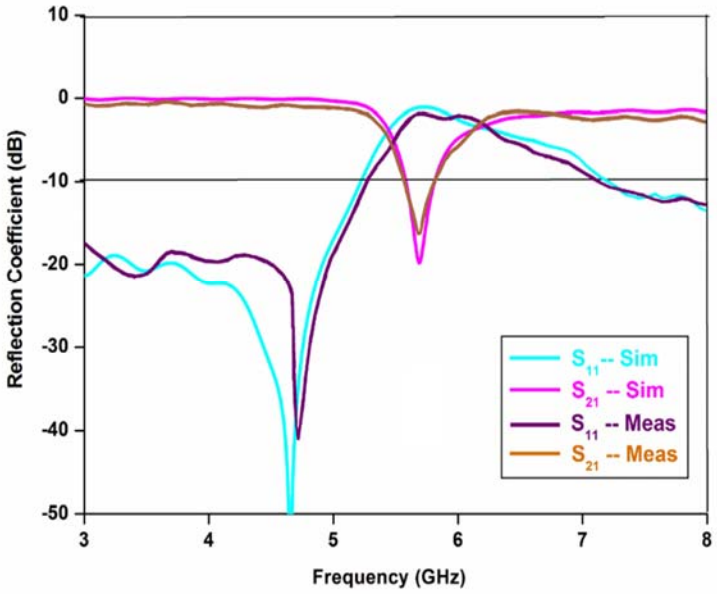

Figure 10. S-parameter (S_{11} and S_{21}) values in simulation and measurement mode.

where

$$\text{Refractive index } (n_{ref}) = (1/k'P_s)\cos^{-1}\left[(1/2S_{21})\left\{(1-S_{11})^2+(S_{21})^2\right\}\right] \quad (10)$$

$$\text{Impedance } (z_s) = \left[\left\{(1+S_{11})^2-(S_{21})^2\right\}/\left\{(1-S_{11})^2-(S_{21})^2\right\}\right]^{1/2} \quad (11)$$

Wave number $k' = 2\pi f/(3\times 10^8\,\text{m/s})$

Slab (substrate material) thickness $= P_s$

The simulated and experimentally extracted S-parameters (S_{21} & S_{11}) of SRR from waveguide environment are illustrated in Figure 10. It is noticed that the transmission peak occurs at resonant frequency 5.75 GHz, which is verified with the theoretical value calculated from Equation (6). Proposed SRR structure works as a magnetically resonator which indicates the negative permeability characteristic at 5.75 GHz because the magnetic field is induced in perpendicular manner. As shown in Figure 10, S_{11} is allocated near zero level (< -2 dB) and S_{21} below -10 dB level at resonant frequency 5.75 GHz, which witnesses stopband characteristics of the proposed SRR at this frequency. The negative permeability feature of the SRR is extracted at 5.75 GHz, as indicated in Figure 11.

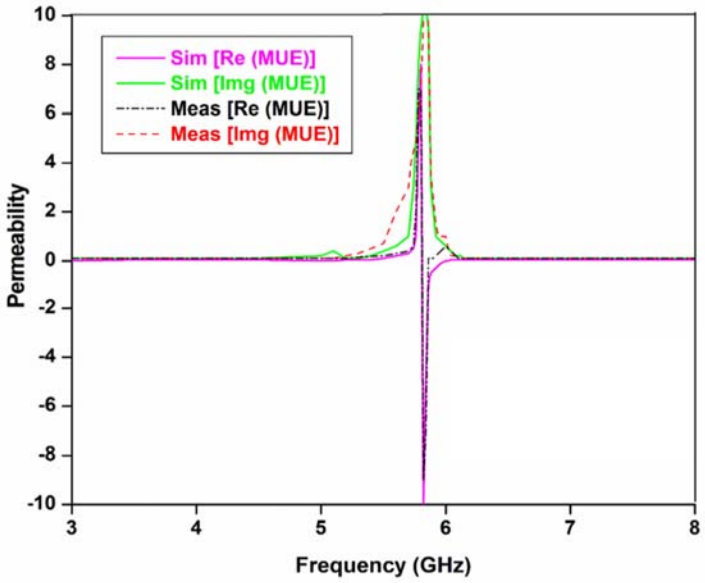

Figure 11. Extracted simulated and measured values of permeability (real and imaginary mue).

3. RESULTS

The simulated surface current distribution of proposed hybrid fractal metamaterial antenna at wireless standards 1.9/3.5/5.8/6.98/10.35/12.5/15.2 GHz is shown in Figure 12. It is noticed that the current exists around the periphery of Moore curve structure connected with feedline and 3rd centered SRR cell in the case of lower resonant frequency (1.98 GHz). For upper resonant band 3.5/5.8 GHz (WiMAX/WLAN), the current spreads out across the surface of the hybrid formatted (Moore and Koch curve) radiating part, which delivers wider bandwidth with improved impedance matching prominent characteristics. Next for higher frequency wireless standards (C/X/KU) at resonant modes of 6.97/10.34/12.54/15.23 GHz, the surface current distribution is extremely identified around the proposed SRR cells as shown in Figure 12. Since for all the resonant modes, current is minimum around the edges of three SRR cells and hybrid radiating part, these represent the improved performance of the proposed design in terms of radiation characteristics as well as reflection coefficient. At higher frequency (above 7 GHz) current is uniformly circulated across the radiating section of antenna, which validates the enhanced impedance matching with wider bandwidth.

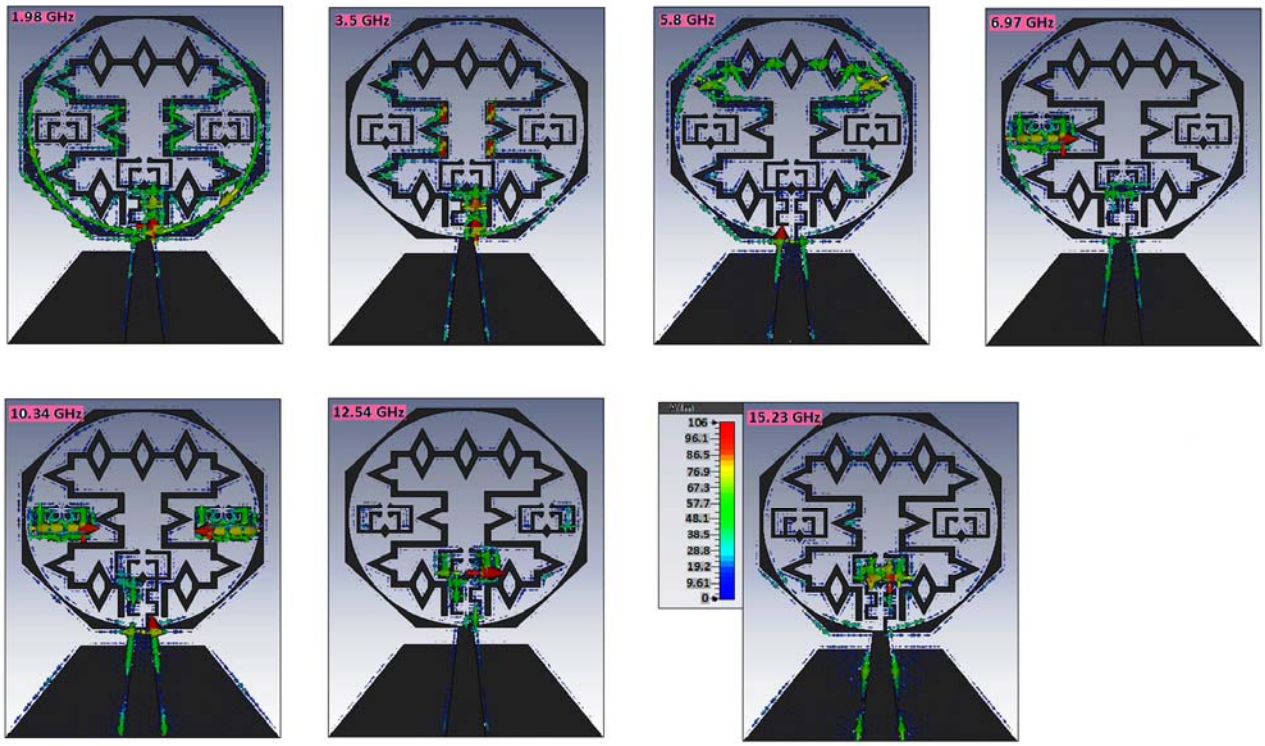

Figure 12. Current distribution (in simulation mode) for hybrid fractal design at 1.98/3.5/5.8/6.97/10.34/12.54/15.23 GHz.

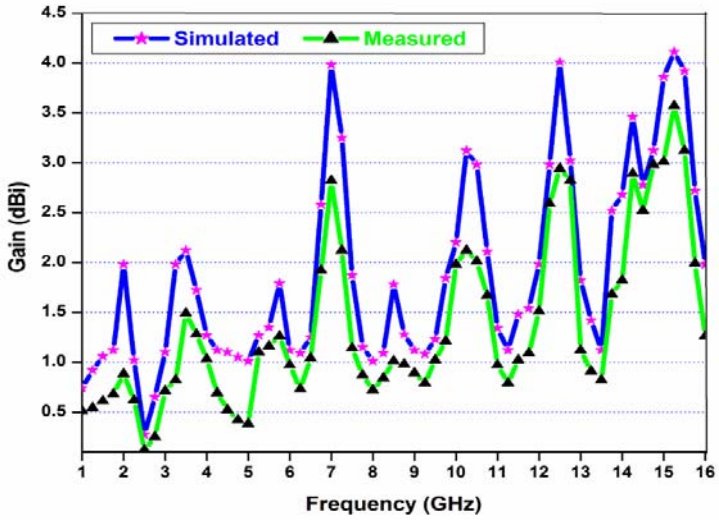

Figure 13. Simulated and experimental antenna gain.

The proposed metamaterial inspired hybrid fractal antenna achieves peak gain of 1.98/2.12/1.79/3.98/3.12-/4.01/4.11 and 0.88/1.49/1.26/2.82/2.12/2.94/3.57 (in dBi) during simulation and experimental mode at resonant frequencies 1.98/3.5/5.8/6.97/10.34/12.54/15.23 (in GHz) respectively as indicated in Figure 13. Another parameter radiation efficiency of the proposed design is observed in Figure 14 in simulation as well as experimental case. The pro-

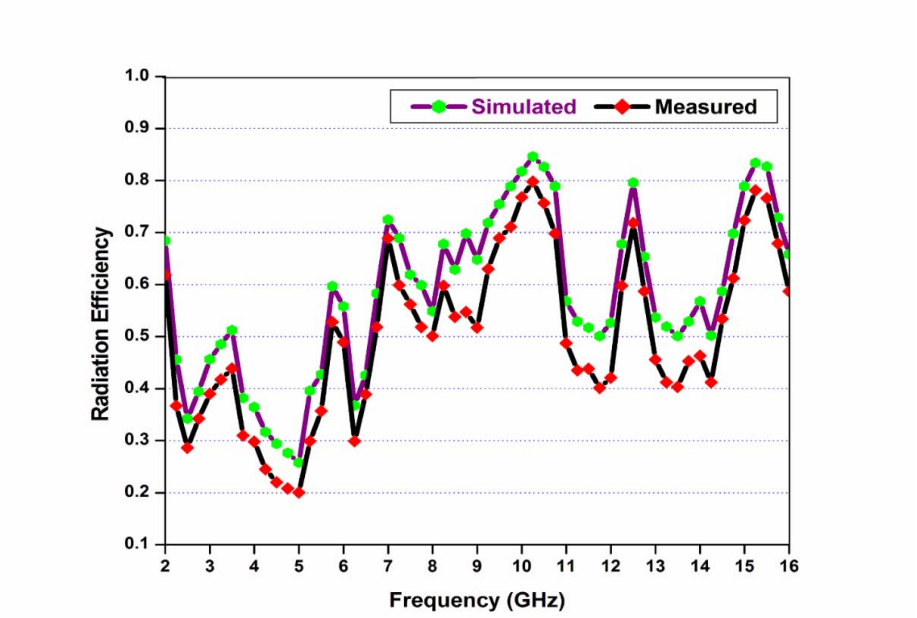

Figure 14. Simulated and experimental antenna radiation efficiency.

posed structure attains radiation efficiencies of 68.45/51.25/59.69/72.45/84.63/79.62/83.41 and 61.82/43.89/52.79/68.91/79.81/71.82/78.11 (in percentage) under simulation and experimental process at wireless standards 1.98/3.5/5.8/6.97/10.34/12.54/15.23 (in GHz), respectively.

For better observation of the proposed design, another parameter radiation patterns are also studied in this section. The patterns are analysed in two principle planes E & H (in co/cross-polarization)

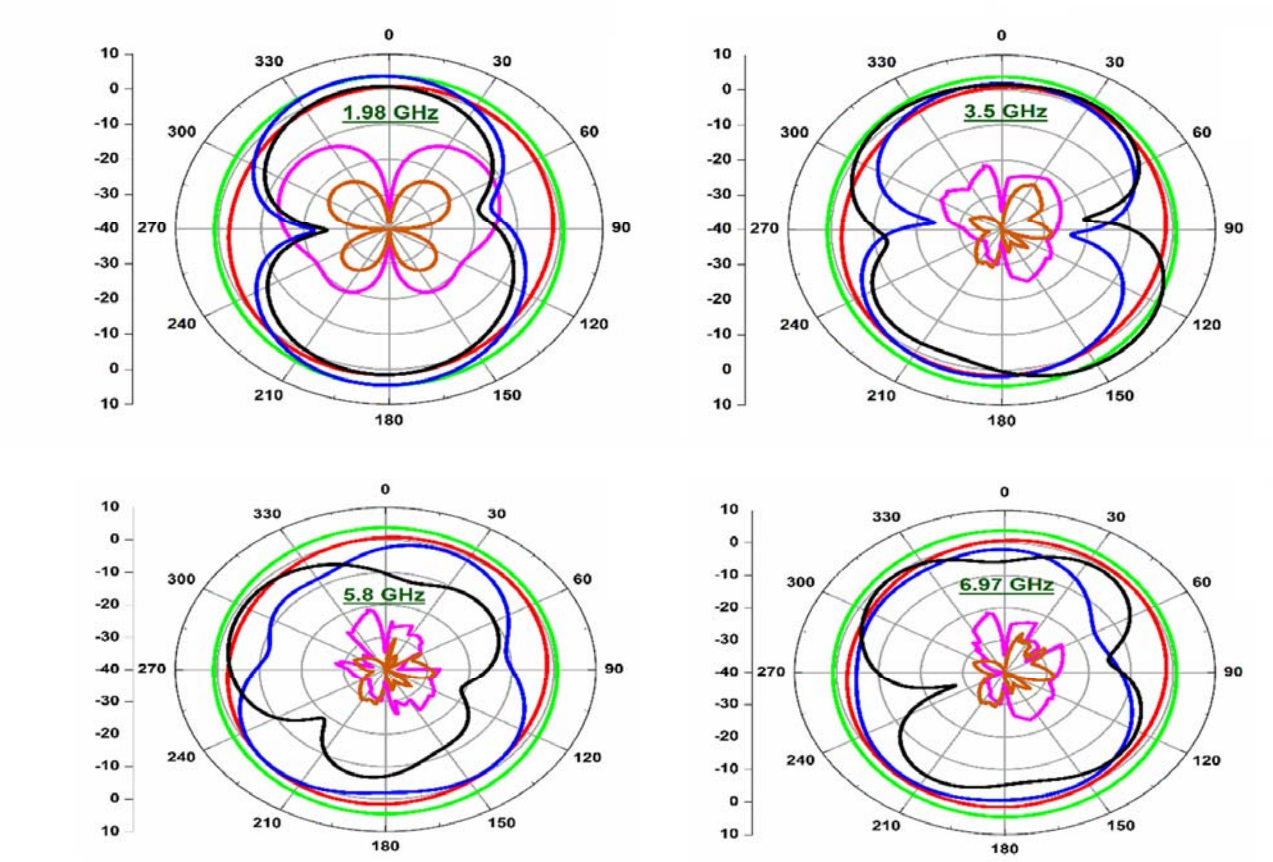

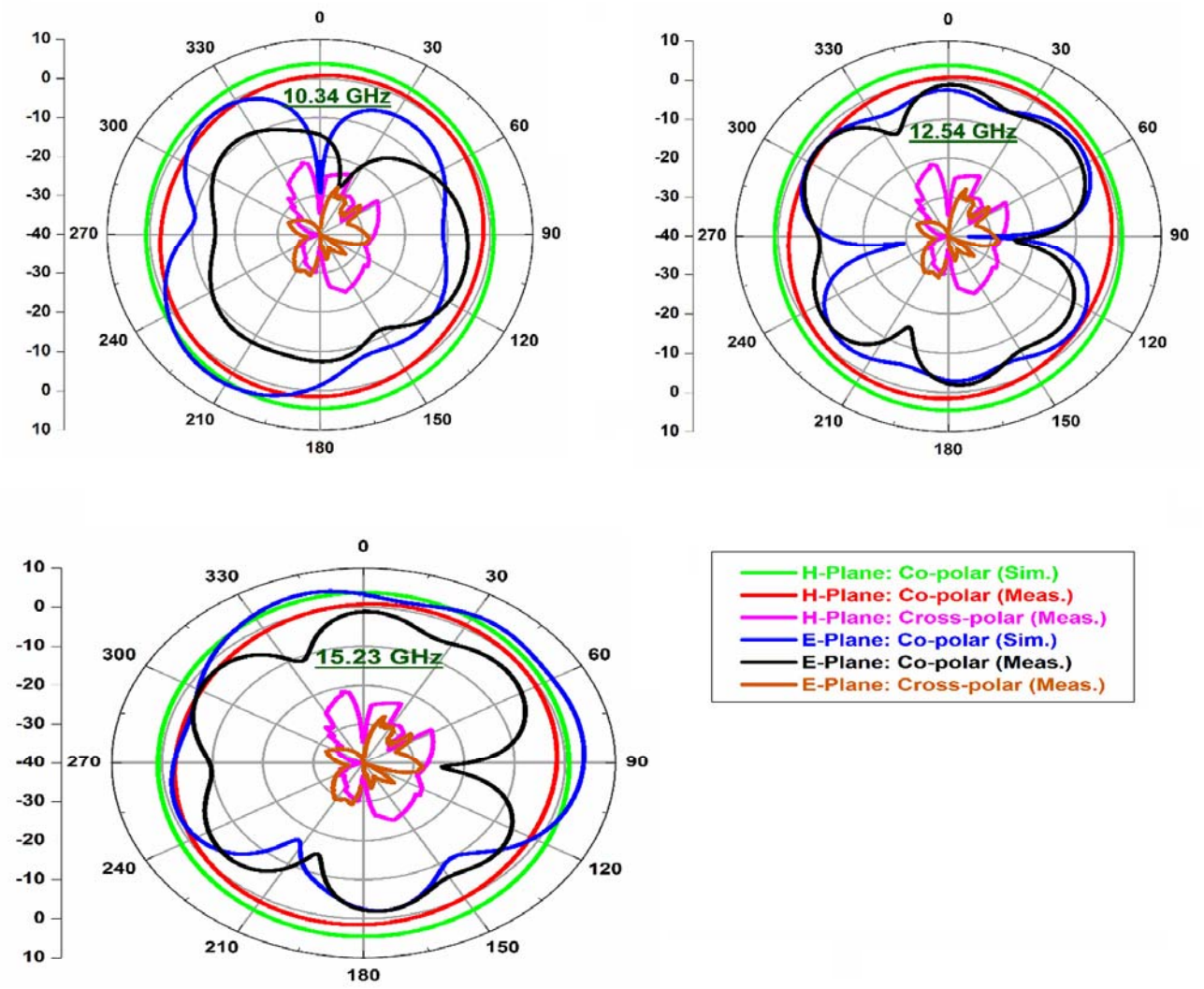

Figure 15. Patterns (E and H in co/cross-polarization mode) of proposed hybrid fractal design at 1.98/3.5/5.8/6.97/10.34/12.54/15.23 GHz.

in simulation as well as measurement mode. There is a good agreement between the two respective mode (simulation/measurement) patterns. Figure 15 represents the comparison of patterns (E and H in co/cross-polarization) of the proposed metamaterial inspired hybrid fractal antenna at distinct resonant frequencies 1.98/3.5/5.8/6.97/10.34/12.54/15.23 GHz. As observed from Figure 15, the patterns are close to omnidirectional and dipole like/bi-directional in H and E planes, respectively, which validate that the proposed structure is good for wireless communication applications. It is further noticed that the patterns are stable with low level of cross polarization (below -15 dB) at all the respective resonant frequencies.

Table 2 delineates the optimality of proposed hybrid fractal antenna with comparison of existing reported designs on the basis of various antenna parameters. Table 2 projects that the proposed structure is novel and useful for covering seven wireless standards as compared to reported multiband antennas.

Table 2. Comparison of proposed structure with reported designs on the basis of antenna parameters.

Ref.	Year	Dimensions (mm × mm ×mm)	Operating bandwidth (%)	Antenna peak gain (dBi)	Antenna radiation efficiency (%)	Resonant bands/ modes	Wireless applications/ Standards (GHz)	Frequency Reconfigurability (PIN diode) approach implemented
[11]	2013	52.6 × 30 ×1	47.27/38.88	−0.56/ − 0.62	89.2/98.1	2	GPS/ WLAN (1.5/2.4)	No
[7]	2014	40 × 40 ×1.6	34.48/18.28/ 19.96	3.97/4.04/ 3.25	−−	3	WLAN/ WiMAX (2.4/3.5/5.8)	No
[5]	2015	56 × 44 ×0.8	5.56/5.86/ 19.34/13.69	1.3/2.3/ 3.5/4.4	76.8/80.1/ 96.6/85.5	4	GPS/WLAN/ WiMAX (1.5/2.4/3.5/5.4)	No
[12]	2016	48 × 48 ×1.6	20.73/15.02/ 31.96	1.64/2.07/ 4.06	66.2/77.15/ 87.6	3	GPS/WLAN (1.9/2.4/5)	No
[13]	2017	19.18 × 22.64 ×1.6	2.4/3.2/ 12.1	1.36/1.57/ 1.83	−−	3	UMTS/WiMAX/ WLAN (2.1/3.45/5.43)	No
[14]	2018	32 × 38 ×1.6	8/6/ 5/69.3	3.8 (Avg. Gain)	89% (Avg. Rad. Eff.)	4	WLAN/WiMAX/ ITU/X Band (2.4/3.35/5.8/7.5)	No
[9]	2018	40 × 40 ×1.5748	15.1/3.45/ 12.59/3.33/ 3.25/5.4/ 16.58	3.48/3.02/ 4.49/4.25/ 3.59/3.81/ 5	−−	7	WLAN/WiMAX/ PAN/OFDM (2.54/3.48/4.02/4.34/ 5.1/5.54/6.24)	No
[23]	2018	30 × 24.8 ×1.6	3.5/5.01/ 13.2/5.77	1.35/1/ 1.07/1.75	−−	4	WiMAX/X Band (3.1/5.52/7.31/9.72)	No
[33]	2019	44 × 39 ×1.6	5.11/7.33/ 11.70/6.38/ 12.03/5.62	2.72/3.81/ 2.12/2.78/ 3.68/4.10	41.2/84.7/ 52.8/69.7/ 78.8/76.9	6	WLAN/WiMAX/ C/X/Ku Band (3.3/5.0/5.8/ 6.6/9.9/15.9)	Yes
[22]	2019	35 × 34 ×1.6	11.81/4.27/ 4.29/6.62/ 3.27/4.22/ 8.13	1.94/2.2/ 1.66/3.87/ 3.65/4.06/ 4.14	41.5/48.6/ 58.1/60.1/ 84.4/78.7/ 82.1	7	WLAN/WiMAX/ C/X/Ku Band (2.4/3/3.5/5/ 5.8/11.8/13.1)	No
Proposed antenna		29.5 × 22 ×1.6	7.48/3.74/ 7.19/13.32/ 25.97/3.92/ 7.26	1.98/2.12/ 1.79/3.98/ 3.12/4.01/ 4.11	68.45/51.25/ 59.69/72.45/ 84.63/79.62/ 83.41	7	Upper L band/ S band WiMAX/ C band WLAN/ C band IEEE INSAT application/ X band/Lower Ku band direct broadcast satellite service/ Middle Ku band satellite communication operating band (1.98/3.5/5.8/6.97/ 10.34/12.54/15.23)	Yes

4. CONCLUSION

A metamaterial inspired hybrid fractal frequency band reconfigurable antenna designed/analysed for Upper L band — 1.98 GHz (Satellite navigation), WiMAX — 3.5 GHz, WLAN — 5.8 GHz, C band — 6.97 GHz (IEEE INSAT application), X band — 10.34 GHz (terrestrial broadband, space communication and Radio Navigation (RN) application), Lower Ku band — 12.54 GHz (direct broadcast satellite service), and Middle Ku band — 15.23 GHz (satellite communication operating band) wireless standards. The radiating part consisting of fusion of Moore curve and Koch curve (single/dual sided) loaded with three metamaterial SRR cells presents the hepta resonating band configuration for wireless applications. The frequency band reconfigurability characteristic for wireless standards is established

by implementation of switching element PIN diode inserted at the center of metallic strip between the Moore curve (adjoined with centered SRR cell) and feedline. The proposed design specifies the radiation patterns with consistency and low cross-polarization, improved and stable gain/radiation efficiency, and good impedance matching at operating wireless communication bands.

ACKNOWLEDGMENT

The author thank Prof. S. K. Koul, CARE, IIT Delhi, India, for providing measurement facilities.

REFERENCES

1. Elsheakh, D. M. N., H. A. Elsadek, E. A. Abdallah, M. F. Iskander, and H. M. S. El-Hennawy, "Reconfigurable single and multiband inset feed microstrip patch antenna for wireless communication devices," *Progress In Electromagnetic Research C*, Vol. 12, 191–201, 2010.
2. Bakariya, P. S., S. Dwari, M. Sarkar, and M. K. Mandal, "Proximity-coupled microstrip antenna for Bluetooth, WiMAX and WLAN applications," *IEEE Antennas and Wireless Propagation Letters*, Vol. 14, 755–758, 2015.
3. Wu, R. Z., P. Wang, Q. Zheng, and R. P. Li, "Compact CPW-fed triple band antenna for diversity applications," *Electron. Letters*, Vol. 51, 735–736, 2015.
4. Mehdipour, A., A. R. Sebak, C. W. Trueman, and T. A. Denidni, "Compact multiband planar antenna for 2.4/3.5/5.2/5.8-GHz wireless applications," *IEEE Antennas and Wireless Propagation Letters*, Vol. 11, 144–147, 2012.
5. Cao, Y. F., S. W. Cheung, and T. I. Yuk, "A multiband slot antenna for GPS/WiMAX/WLAN systems," *IEEE Transactions on Antennas and Propagation*, Vol. 63, No. 3, 952–958, 2015.
6. Saraswat, R. K. and M. Kumar, "A frequency band reconfigurable UWB antenna for high gain applications," *Progress In Electromagnetics Research B*, Vol. 64, 29–45, 2015.
7. Samsuzzaman, M., T. Islam, N. H. Abd Rahman, M. R. I. Faruque, and J. S. Mandeep, "Compact modified Swastika shape patch antenna for WLAN/WiMAX applications," *International Journal of Antennas and Propagation*, Vol. 2014, 1–8, 2014.
8. Ali, T., S. Pathan, and R. C. Biradar, "A multiband antenna loaded with metamaterial and slots for GPS/WLAN/WiMAX applications," *Microwave and Optical Technology Letters*, Vol. 60, 79–85, 2018.
9. Chaurasia, P., B. K. Kanaujia, S. Dwari, and M. K. Khandelwal, "Design and analysis of seven-bands-slot-antenna with small frequency ratio for different wireless applications," *Int. J. Electron. and Commun. (AEÜ)*, Vol. 99, 100–109, 2018.
10. Zhu, J. and G. V. Eleftheriades, "Dual band metamaterial inspired small monopole antenna for WiFi applications," *Electron. Letters*, Vol. 45, No. 22, 1104–1106, 2009.
11. Xu, H.-X., G.-M. Wang, Y.-Y. Lv, M.-Q. Qi, X. Gao, and S. Ge, "Multifrequency monopole antennas by loading metamaterial transmission lines with dual-shunt branch circuit," *Progress In Electromagnetics Research*, Vol. 137, 703–725, 2013.
12. Alam, T., M. Samsuzzaman, M. R. I. Faruque, and M. T. Islam, "A metamaterial unit cell inspired antenna for mobile wireless applications," *Microwave and Optical Technology Letters*, Vol. 58, No. 2, 263–267, 2016.
13. Daniel, S., R. Pandeeswari, and S. Raghavan, "A compact metamaterial loaded monopole antenna with offset-fed microstrip line for wireless applications," *Int. J. Electron. and Commun. (AEÜ)*, Vol. 83, 88–94, 2017.
14. Rao, M. V., B. T. P. Madhav, T. Anilkumar, and B. P. Nadh, "Metamaterial inspired quad band circularly polarized antenna for WLAN/ISM/Bluetooth/WiMAX and satellite communication applications," *Int. J. Electron. and Commun. (AEÜ)*, Vol. 97, 229–241, 2018.
15. Anguera, J., C. Puente, C. Borja, and J. Soler, "Fractal shaped antennas: A review," *Encyclopedia of RF and Microwave Engineering*, Wiley Interscience, 2005.

16. Chen, H. D., H. W. Yang, and C. Y. D. Sim, "Single open-slot antenna for LTE/WWAN smartphone application," *IEEE Transactions on Antennas and Propagation*, Vol. 65, No. 8, 4278–4282, 2017.
17. Lee, S. H., Y. Lim, Y. J. Yoon, C. B. Hong, and H. I. Kim, "Multiband folded slot antenna with reduced hand effect for handsets," *IEEE Antennas and Wireless Propagation Letters*, Vol. 9, 674–677, 2010.
18. Yuan, B., Y. Cao, and G. Wang, "A miniaturized printed slot antenna for six-band operation of mobile handsets," *IEEE Antennas and Wireless Propagation Letters*, Vol. 10, 854–857, 2011.
19. Sharma, S. K., J. D. Mulchandani, D. Gupta, and R. K. Chaudhary, "Triple band metamaterial inspired antenna using FDTD technique for WLAN/WiMAX applications," *International Journal of RF and Microwave Computer-Aided Engineering*, Vol. 25, No. 8, 688–695, 2015.
20. Ali, T. and R. C. Biradar, "A compact multiband antenna using $\lambda/4$ rectangular stub loaded with metamaterial for IEEE 802.11 N and IEEE 802.16 E," *Microwave and Optical Technology Letters*, Vol. 59, No. 5, 1000–1006, 2017.
21. Kukreja, J., D. Kumar Choudhary, and R. Kumar Chaudhary, "CPW fed miniaturized dual-band short-ended metamaterial antenna using modified split-ring resonator for wireless application," *International Journal of RF and Microwave Computer-Aided Engineering*, Vol. 27, No. 8, 1–7, 2017.
22. Saraswat, R. K. and M. Kumar, "A metamaterial hepta-band antenna for wireless applications with specific absorption rate reduction," *International Journal of RF and Microwave Computer-Aided Engineering*, Vol. 29, No. 10, 1–12, 2019.
23. Ali, T., A. M. Saadh, and R. C. Biradar, "A fractal quad-band antenna loaded with L-shaped slot and metamaterial for wireless applications," *International Journal of Microwave and Wireless Technologies*, Vol. 10, No. 7, 826–834, 2018.
24. Pandeeswari, R. and S. Raghavan, "Broadband monopole antenna with split ring resonator loaded substrate for good impedance matching," *Microwave and Optical Technology Letters*, Vol. 56, No. 10, 2388–2392, 2014.
25. Arora, C., S. S. Pattnaik, and R. N. Baral, "SRR inspired microstrip patch antenna array," *Progress In Electromagnetics Research C*, Vol. 58, 89–96, 2015.
26. Rajeshkumar, V. and S. Raghavan, "SRR based polygon ring penta-band fractal antenna for GSM/WLAN/WiMAX/ITU band applications," *Microwave and Optical Technology Letters*, Vol. 57, No. 6, 1301–1305, 2015.
27. Elavarasi, C. and T. Shanmuganantham, "Multiband SRR loaded Koch star fractal antenna," *Alexandria Engg. J.*, Vol. 57, No. 3, 1549–1555, 2018.
28. Ahmed, B.-H. and Nrnikman, "Fractal microstrip antenna with Minkowski island split ring resonator for broad band application," *IEEE Int. RF and Micro. Conf.*, 2013, doi.org/10.1109/RFM.2013.6757252.
29. Hu, J.-R. and J.-S. Li, "Compact microstrip antennas using SRR structure ground plane," *Microwave and Optical Technology Letters*, Vol. 56, No. 1, 117–120, 2014.
30. Rajkumar, R. and K. Usha Kiran, "A metamaterial inspired compact open split ring resonator antenna for multiband operation," *Wireless Personal Communications*, Vol. 97, 951–965, 2017.
31. Rajeshkumar, V. and S. Raghavan, "A compact metamaterial inspired triple band antenna for reconfigurable WLAN/WiMAX applications," *Int. J. Electron. Commun.*, Vol. 69, No. 1, 274–280, 2015.
32. Saraswat, R. K. and M. Kumar, "Miniaturized slotted ground UWB antenna loaded with metamaterial for WLAN and WiMAX applications," *Progress In Electromagnetics Research B*, Vol. 65, 65–80, 2016.
33. Saraswat, R. K. and M. Kumar, "A vertex-fed hexa-band frequency reconfigurable antenna for wireless applications," *International Journal of RF and Microwave Computer-Aided Engineering*, Vol. 29, No. 10, 1–13, 2019.
34. Liu, W. C., C. M. Wu, and Y. Dai, "Design of triple-frequency microstrip-fed monopole antenna using defected ground structure," *IEEE Transactions on Antennas and Propagation*, Vol. 59, No. 7,

2457–2463, 2011.

35. Balanis, C. A., *Antenna Theory: Analysis and Design*, Wiley Inter Science, Hoboken, NJ, 2005.
36. Naqvi, A., M. S. Khan, and B. D. Braaten, "A frequency reconfigurable cylindrically shaped surface with cloaking-like properties," *Microwave and Optical Technology Letters*, Vol. 58, No. 6, 1323–1329, 2016.
37. Naqvi, S. A. and M. S. Khan, "Design of a miniaturized frequency reconfigurable antenna for rectenna in WiMAX and ISM frequency bands.," *Microwave and Optical Technology Letters*, Vol. 60, No. 2, 325–330, 2018.
38. Computer simulation technology microwave studio (CST MWS). Retrieved from http://www.cst.co.
39. Alpha Industries. ALPHA-6355 beamlead PIN diode. Data sheet 2014 [Online]. Available: http://www.datasheetarchive.com/ALPHA/PINdiode6355-datasheet.html.
40. Kumar, Y. and S. Singh, "A compact multiband hybrid fractal antenna for multistandard mobile wireless application," *Wireless Personal Communications*, Vol. 84, 57–67, 2015.
41. Chen, H., J. Zhang, Y. Bai, Y. Luo, L. Ran, Q. Jiang, et al., "Experimental retrieval of the effective parameters of metamaterials based on a waveguide method," *Opt. Express*, Vol. 14, No. 26, 12944–12949, 2006.
42. Saha, C. and J. Y. Siddiqui, "Versatile CAD formulation for estimation of the resonant frequency and magnetic polarizability of circular split ring resonators," *International Journal of RF and Microwave Computer-Aided Engineering*, Vol. 21, 432–438, 2011.
43. Smith, D. R., S. Schultz, P. Markos, and C. M. Soukoulis, "Determination of negative permittivity and permeability of metamaterials from reflection and transmission coefficients," *Phys. Rev. B.*, Vol. 65, 195104–195109, 2002.
44. Saha, C. and J. Y. Siddiqui, "Versatile CAD formulation for estimation of the resonant frequency and magnetic polarizability of circular split ring resonators," *International Journal of RF and Microwave Computer-Aided Engineering*, Vol. 21, 432–438, 2011.
45. Dwivedi, S. K., M. Kumar, and L. Tharani, "A rectangular SRR switched slotted microstrip patch for frequency diversity application," *Wireless Personal Communications*, Vol. 103, No. 4, 2863–2875, 2018.